

ECG Classification based on Wasserstein Scalar Curvature

Fupeng Sun, Yin Ni, Yihao Luo, Huafei Sun*

Abstract: Electrocardiograms (ECG) analysis is one of the most important ways to diagnose heart disease. This paper proposes an efficient ECG classification method based on Wasserstein scalar curvature to comprehend the connection between heart disease and mathematical characteristics of ECG. The newly proposed method converts an ECG into a point cloud on the family of Gaussian distribution, where the pathological characteristics of ECG will be extracted by the Wasserstein geometric structure of the statistical manifold. Technically, this paper defines the histogram dispersion of Wasserstein scalar curvature, which can accurately describe the divergence between different heart diseases. By combining medical experience with mathematical ideas from geometry and data science, this paper provides a feasible algorithm for the new method, and the theoretical analysis of the algorithm is carried out. Digital experiments on the classical database with large samples show the new algorithm's accuracy and efficiency when dealing with the classification of heart disease.

keywords: ECG Classification, Positive definite symmetric matrix manifold, Wasserstein metric, Curvature

1 Introduction

As one of the most common and deadly diseases in the world, heart disease poses a significant threat to people's happiness and healthy life. With the increase of social pressure, the incidence of heart disease is proliferating in recent years [1]. Therefore, it is of great indispensability to realize the efficient diagnosis, real-time monitoring and prediction for heart disease. At present, the diagnosis is mainly made through doctors' manual analysis of ECG (electrical activity records of patient's heart contraction) [2]. With no exception, ECG analysis requires doctors to command professional and detailed medical knowledge. However, as a kind of valuable medical resource, the distribution

*This research was funded by National Key Research and Development Plan of China, No. 2020YFC2006201

of experienced doctors is not well balanced in different regions of the world. Thus, the life and health of patients can not be fully protected in the situation with poor medical conditions and resources.

With the rapid development of computer technology, using computer-aided diagnosis technology to screen heart diseases has become a new technical method to alleviate the imbalance of artificial medical resources. The normal ECG shows regular changes of PQRST complex [3], and different pathological features will cause symmetry vanishing. The computer-aided diagnosis techniques aim to extract different features of ECG and detect fluctuation of PQRST complex in the view of these features to achieve accurate classification.

Commonly used computer-aided diagnosis techniques mainly extract features from the viewpoints of signal analysis, dynamic system modeling (DSA) and topological data analysis (TDA), which are also combined with classic statistical analysis [14] and machine learning [15–17]. Signal analysis can directly extract morphological features such as amplitude [4, 5] or use wavelet transform to acquire frequency domain features [6, 7]. Other emerging signal analysis methods [8] also have the potential to analyze ECG. Dynamical system analysis is used to model cardiac dynamical system through phase space reconstruction [9–13]. Topological data analysis transforms ECG signals into point clouds by time-delay embedding or Fourier transform, and then extracts topological features from point clouds [18–23]. Above mentioned methods are adaptive with different applied conditions. Despite various advantages of conventional methods, most of them are limited by small sample size or poor interpretation. Thus a new way without such limitations need to be proposed.

Inspired by persistent homology (PH) [24] in TDA, a geometric data analysis method is proposed and applied to ECG classification. PH transforms the original ECG signals into point clouds in Euclidean space by embedding in a suitable way and extracts topological features from point clouds. Topological features can reflect different pathological characteristics of the original ECG, so as to realize the classification. But the topological characteristics cannot focus on fine local information of point clouds, also the category number and sample size are limited. Thus, it is necessary to describe the local differences of point clouds in a more accurate method.

Each point of the point cloud in n dimensional Euclidean obtained by Fast Fourier transform embedding (FFT embedding) [23] is mapped to a n dimensional Gaussian

distribution by local statistic, that is, the point cloud in Euclidean space is transformed into the point cloud on the positive definite symmetric matrix manifold $SPD(n)$. $SPD(n)$ becomes a Riemannian manifold after being endowed with the natural Riemannian metric induced by Wasserstein distance [25]. We reveal the local differences of point clouds on $SPD(n)$ [27] by Wasserstein scalar curvature (WSC). By analyzing Wasserstein scalar curvature histogram (WSCH) of the converted point clouds, we originally defined a new data characteristic, called Wasserstein scalar curvature dispersion (WSCD) which can express the pathological changes of heart. Finally, the ECG classification algorithm based on Wasserstein scalar curvature (WSCEC) is designed to classify ECG signals.

This paper is organized as follows. Section 2 gives the preliminaries. Section 3 presents WSCEC algorithm. In Section 4, we analyze the numerical results. Finally, we discuss the main conclusions and prospects for the future research in Section 5.

2 Preliminaries

In this section, we will introduce some basic preliminaries such as FFT embedding, local statistic and Wasserstein geometric structure on $SPD(n)$.

2.1 Fast Fourier transform embedding

Fourier transform decomposes signals into waves with different frequencies and reveals the certain features hidden in the time domain. For discrete inputs, fast Fourier transform (FFT) is a widely used tool. Given a signal $T = \{t_i\}_{i=1}^n$ with even n , t_i can be represented as:

$$t_i = \frac{1}{n} \sum_{k=0}^{n-1} C_k e^{j \frac{2\pi}{n} k i}, \quad (1)$$

where $C_k = \sum_{i=0}^{n-1} t_i e^{-j \frac{2\pi}{n} k i}$.

Let $C_k = a_k + b_k j$, then we have $C_{n-k} = a_k - b_k j$ and

$$C_k e^{j \frac{2\pi}{n} k i} + C_{n-k} e^{j \frac{2\pi}{n} (N-k) i} = A_k \cos \left(\frac{2\pi k i}{n} + \phi_k \right), \quad (2)$$

where $A_k = 2\sqrt{a_k^2 + b_k^2}$, $\tan(\phi_k) = \frac{b_k}{a_k}$.

If the sample frequency is f_s , by combining equation (1) and equation (2), we have

$$t(s) = \frac{1}{n} \sum_{k=0}^{\frac{n}{2}-1} A_k \cos \left(f_s \frac{2\pi k s}{n} + \phi_k \right), \quad (3)$$

where $t_i = t \left(\frac{i}{f_s} \right)$.

Now we use FFT and sliding windows to convert signal $T = \{t_i\}_{i=1}^n$ to a point cloud in \mathbb{R}^d . Let l be window length and τ be sliding speed. Firstly, we transform T into a signal set $\mathcal{P}_{l,\tau}(T) = \{p_k\}_{k=1}^{\hat{n}-1}$ with $\hat{n} = \lfloor \frac{n-l}{\tau} \rfloor$ and $p_k = [t_{k\tau}, t_{k\tau+1}, \dots, t_{k\tau+(l-1)}]$. Secondly, we transform each p_k into a point in \mathbb{R}^d by choosing the first d bases from FFT and obtain the following point cloud:

$$T \rightarrow \mathcal{P}_{l,\tau}(T) = \{p_k\}_{k=1}^{\hat{n}-1} \rightarrow S_F(T) = S_{l,\tau,d}(T) = \left\{ \frac{2}{l} \left(a_0^k, a_1^k, b_1^k, \dots, a_{\frac{d}{2}-1}^k, b_{\frac{d}{2}-1}^k \right) \right\}_{k=1}^{\hat{n}-1}. \quad (4)$$

where $d \leq l$.

2.2 Local statistic

Objective phenomena in nature are often disturbed by many small random variables, which assigns a random distribution with the local neighborhood of any point in the point cloud. If the factors which affect the local distribution of a point cloud are considered small and complex enough, then according to the law of large numbers and the central limit theorem, we can assume that the local statistic comes from a high-dimensional Gaussian distribution whose parameters are neighborhood mean and neighborhood covariance matrix.

In data science, kNN algorithm provides a natural neighborhood selection method. The idea is to search for the nearest k points as the neighborhood samples of any fixed point in the point cloud. To acquire local statistic, for every point $P_i \in S_F(T)$, we can search kNN to obtain neighborhood $\mathcal{N}_i = \{N_{ij} | j = 1, \dots, k\}$, and calculate local mean μ_i and covariance matrix Σ_i :

$$\mu_i = \frac{1}{k} \sum_{j=1}^k N_{ij}, \quad \Sigma_i = \sum_{j=1}^k (N_{ij} - \mu_i)^T (N_{ij} - \mu_i). \quad (5)$$

Consequently, $S_F(T)$ is converted to a point cloud in $SPD(d)$:

$$S_F(T) \rightarrow S_P(T) = S_{SPD}(T, k) = \{\Sigma_i | P_i \in S_F(T)\}. \quad (6)$$

2.3 Wasserstein geometric structure on $SPD(n)$

Wasserstein distance describes the minimal energy used to transport one distribution to another. It can be used to measure the difference between two distributions and is vividly called earth-moving distance [25].

Let F_1, F_2 be two distributions. Then the Wasserstein distance between F_1 and F_2 is defined as the infimum of geodesic distance integral needed for transporting probability measure element:

$$W_p(F_1, F_2) = \inf_{p \sim \Pi(F_1, F_2)} \left(E_{(x,y) \sim p} [\|x - y\|^p] \right)^{\frac{1}{p}}, \quad (7)$$

where $\Pi(F_1, F_2)$ is the set of joint distributions taking F_1, F_2 as marginal distributions, E is the expectation.

Although the definition is abstract and there is no explicit expression for the general Wasserstein distance, the Wasserstein distance between any two Gaussian distributions in \mathbb{R}^n has the following explicit expression [28]:

$$W(\mathcal{N}_1, \mathcal{N}_2) = \|\mu_1 - \mu_2\| + \left(\text{tr} \left(\Sigma_1 + \Sigma_2 - 2(\Sigma_1 \Sigma_2)^{\frac{1}{2}} \right) \right)^{\frac{1}{2}}, \quad (8)$$

where μ_i and Σ_i are the mean and covariance matrix of Gaussian distribution \mathcal{N}_i , $i = 1, 2$.

Wasserstein distance can be induced by a Riemannian metric on $SPD(n)$ defined as:

$$g_W|_S(X, Y) = \frac{1}{2} \text{tr}(\Gamma_S[Y]X), \quad (9)$$

where $S \in SPD(n)$, $X, Y \in T_S SPD(n)$ are tangent vectors and $\Gamma_S[Y]$ is the solution of Sylvester equation $S\Gamma_S[Y] + \Gamma_S[Y]S = Y$ [30].

Because the geodesic distance induced by the equation (9) is consistent with the original definition of Wasserstein distance (8), we call g_W Wasserstein metric. In addition, we write the Riemannian manifold $SPD(n)$ endowed with Wasserstein metric as $(SPD(n), g_W)$.

For any $S \in (SPD(n), g_W)$, let X, Y be the smooth vector field of $SPD(n)$. [26, 27] provide the explicit expression of Riemannian curvature tensor $\langle R_{XY}X, Y \rangle$ at S :

$$R(X, Y, X, Y) = 3\text{tr}(\Gamma_S[X]S\Gamma_S(\Gamma_S[X]\Gamma_S[Y] - \Gamma_S[Y]\Gamma_S[X])S\Gamma_S[Y]). \quad (10)$$

Furthemore, the scalar curvature at S satisfies

$$\begin{aligned} \rho(S) &= \sum_{i=1}^n \sum_{j=1}^n R(e_i, e_j, e_i, e_j) \\ &= 3\text{tr}(U\Lambda(U + U^T) + (U + U^T)\Lambda U + (U + U^T)\Lambda U\Lambda(U + U^T)), \end{aligned} \quad (11)$$

where $\{e_i\}$ is any standard orthonormal basis of $T_S SPD(n)$, $\Lambda = \text{diag}(\lambda_1, \dots, \lambda_n)$ is orthogonal similar to S , λ_i is the i th eigenvalue of S , and $U = \left[\frac{1}{\lambda_i + \lambda_j} \right]_{i < j}$ is an upper triangular matrix.

Note that the scalar curvature of S can be controlled by the second small eigenvalue of S . Actually, there exists a standard orthonormal basis $\{e_k\}$ of $T_S SPD(n)$, such that $\forall e_{k_1}, e_{k_2} \in \{e_k\}$,

$$0 < K_S(e_{k_1}, e_{k_2}) = \sum_{j=1}^n R(e_{k_1}, e_{k_j}, e_{k_2}, e_{k_j}) < \frac{3}{\lambda_{min2}(S)}, \quad (12)$$

where λ_{min2} is the second small eigenvalue of S .

Furthermore, by equation (11), we have

$$0 < \rho(A) < \frac{3n(n-1)}{\lambda_{min2}(S)}. \quad (13)$$

The boundedness of WSC indicates that the curvature of local covariance matrix is controllable unless the local covariance degenerates in two dimensions or more. Consequently, for most neighborhoods, as long as using appropriate embedding methods to make sure there is no degeneration beyond two dimensions, WSC of point cloud on $SPD(n)$ will be in a controllable range, which provides a theoretical criterion for the robustness of our algorithm.

3 ECG Classification Algorithm based on Wasserstein Scalar Curvature

In this section, we will introduce WSCEC algorithm which can detect the heart disease. Wasserstein scalar curvature dispersion is extracted to reveal the change of regularity of PQRST complex. The framework of WSCEC algorithm is as follows.

- Continuous ECG signals are segmented and denoised by interpolation and filter to obtain multiple single heartbeats.
- Every single ECG is transformed into a point cloud in Euclidean space by FFT embedding. Through local statistic, the point cloud in Euclidean space is converted to the point cloud on $SPD(n)$.
- Calculate WSC of each point to obtain WSCH and extract WSCD as the feature.
- Do auxiliary diagnosis according to clustering results.

The intuitive algorithm pipeline is shown in Figure 1.

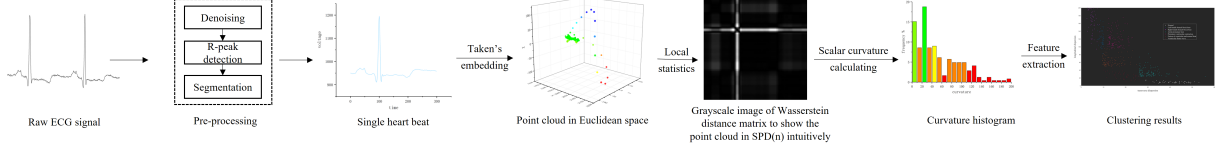


Figure 1: Pipeline of WSCEC

3.1 Preprocessing of ECG signal

We adopt the idea of Butterworth filter algorithm [29] to cut off noisy portions with spectral power over 50 Hz. By developing a local search algorithm to find the periodic R-peak in PQRST complex, we successfully transform continuous ECG signals into multiple single heartbeats with length 300.

Noting that the length of the sharp part of QRS complex in normal ECG is around 10, we set window length $l = 10$ and sliding speed $\tau = 1$ to emphasize the change of QRS complex when sliding the window. Then by using equation (4) and taking $d = 3$, we convert various single heartbeats to point clouds in \mathbb{R}^3 . Let T_s be a standard normal ECG signal, denote $S_F(T_s)$ as the Euclidean point cloud of T_s after FFT embedding. Figure 2 shows $S_F(T_s)$ intuitively.

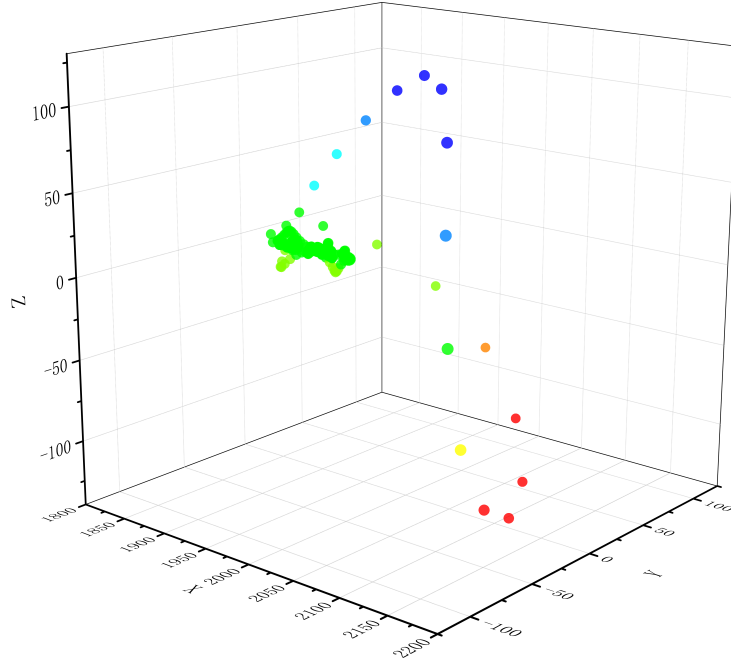


Figure 2: Point cloud of T_s in \mathbb{R}^3 after FFT embedding

In attempt to describe the local differences of Euclidean point clouds more accurately, we obtain neighborhood properties by local statistic. We combine kNN algorithm with



Figure 3: Grayscale image of Wasserstein distance matrix for point cloud of T_s on $SPD(3)$

equation (5) to obtain $S_P(T_s)$, the parameter of kNN algorithm is $k = 20$. With an attempt to give readers an intuitive understanding of the structure of point clouds on $SPD(3)$, we acquire Wasserstein distance matrices by equation (8) and present the grayscale images of Wasserstein distance matrix for T_s , see Figure 3.

3.2 Feature extraction

The pathological differences of original ECG signals are completely reflected by the local information of point clouds, and the differences of local information are further reflected in the neighborhood mean and covariance matrix, that is, reflected in the point-by-point difference of point clouds on $SPD(n)$. Since Wasserstein scalar curvature reflects the structural relationship between a point and its adjacent points, we can use WSC to describe different pathological features of ECG signals.

Firstly, we calculate WSC of each point in the distribution point cloud, then the corresponding WSC sequence $\mathcal{W} = \{w_i\}_{i=1}^{\hat{n}}$ can be obtained. Furthermore, we can acquire WSCH:

$$H(m, b) = \left\{ ([mj, m(j+1)), y_j) \mid 0 \leq j \leq \left\lfloor \frac{b}{m} \right\rfloor \right\}, \quad (14)$$

where

$$y_j = |\{w_k \in \mathcal{W} \mid mk \leq w_k < m(k+1)\}|, \quad (15)$$

$[\cdot]$ denotes integer operator and $|\cdot|$ denotes the cardinality or size of a finite set.

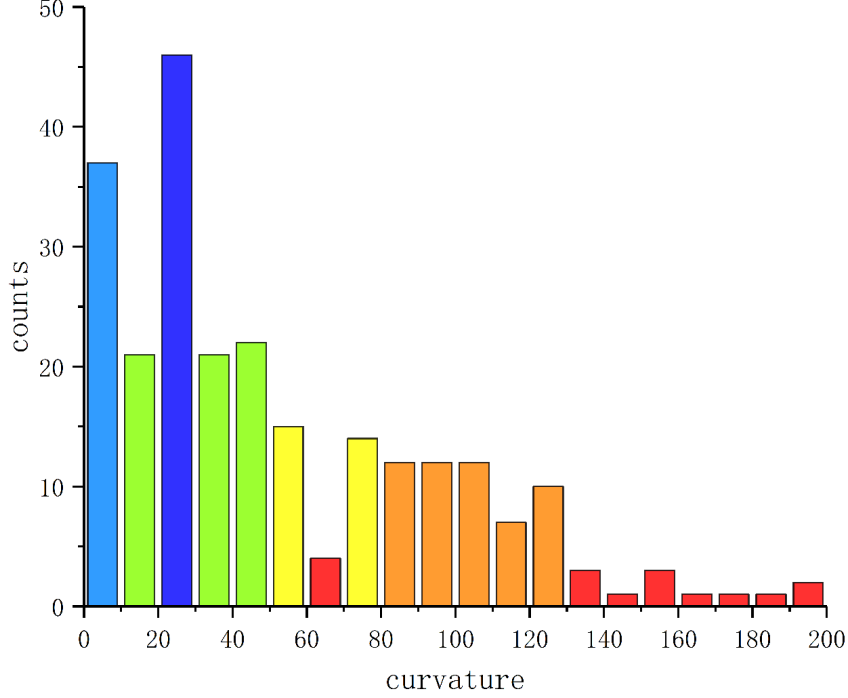


Figure 4: WSCH for distribution point cloud of T_{STD}

Figure 4 performs the WSCH of the point cloud $S_P(T_s)$ on $SPD(3)$ where $m = 10, b = 200$. Now we give the definition of WSCD to describe the differences of WSC sequence.

Definition 1 For the given WSC sequence \mathcal{W} , its histogram $H(m, b)$ and $0 \leq s \leq \lfloor \frac{b}{m} \rfloor$ ($s \in \mathbb{N}_+$), define:

$$\begin{aligned} cur_1(m, b, s) &= \text{median of } \mathcal{U}_1, \\ cur_2(m, b, s) &= \frac{1}{|\mathcal{U}_2| - s - 1} \sum_{j \geq s+1} \left(y_j - \frac{\sum_{j \in \mathcal{U}_2} y_j}{\lfloor \frac{b}{m} \rfloor} \right)^2, \\ cur(m, b, s) &= (cur_1(m, b, s), cur_2(m, b, s)), \end{aligned} \quad (16)$$

where

$$\begin{aligned} \mathcal{U}_1 &= \{w_k \in \mathcal{W} \mid ms \leq w_k \leq b\}, \\ \mathcal{U}_2 &= \{k \geq s+1 \mid y_k \neq 0\}. \end{aligned} \quad (17)$$

We call $cur_1(m, b, s)$ Wasserstein scalar curvature transverse dispersion of \mathcal{W} , $cur_2(m, b, s)$ Wasserstein scalar curvature longitudinal dispersion of \mathcal{W} and $cur(m, b, s)$ Wasserstein scalar curvature dispersion of \mathcal{W} , respectively.

In histogram $H(m, b)$, transverse dispersion $cur_1(m, b, s)$ is the median of the intersection between \mathcal{W} and $[ms, b]$. $cur_1(m, b, s)$ describes the homogeneity of \mathcal{W} ranging in $[m(s + 1), b]$ horizontally.

The longitudinal dispersion $cur_2(m, b, s)$ represents the fluctuation of the column, which can be regarded as the correction of the standard deviation. If the column heights of some curvature intervals in $H(m, b)$ are 0, then this fluctuation is further amplified. $cur_2(m, b, s)$ describes the uniformity of \mathcal{W} ranging in $[m(s + 1), b]$ vertically. In particular, $cur_2(m, b, 0)$ is the standard deviation of the curvature histogram $H(m, b)$ if the columns are all nonzero.

Therefore, $cur(m, b, s)$ describes the homogeneity of \mathcal{W} overall, $cur(m, b, s)$ is closer to $(\frac{1}{2}(b + ms), 0)$ if the columns are more evenly distributed. Since the ECG of healthy heartbeats have strong regularity, their WSCD are more even, as shown in Figure 5. We consider WSCD $cur(m, b, s)$ as the feature of our final classification.

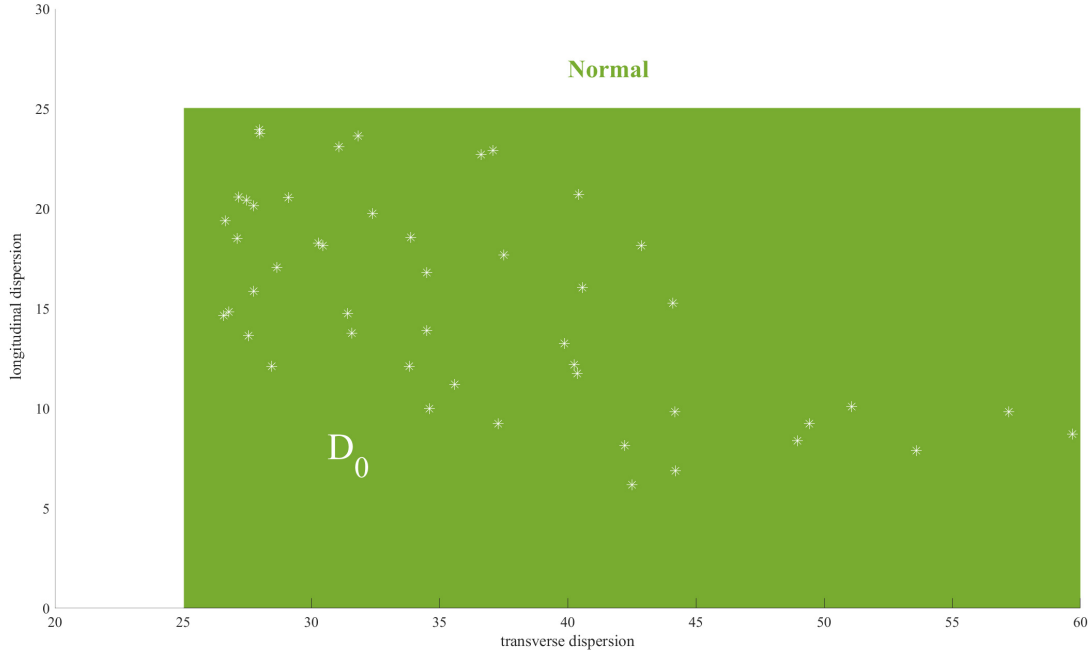


Figure 5: WSCD of normal ECG signals

3.3 Case analysis

Figure 6 shows seven types of single heartbeats. Compared with normal ECG signal, other six diseases have different effects on PQRST complex. The QRS complex of left bundle branch block heartbeats (L. B. B. B.) or right bundle branch block heartbeats (R. B. B. B.) is obviously broadened, and generally there are two R peaks. The P wave of atrial premature heartbeats (A. P.) occurs earlier and is significantly different from that of sinus. P. V. C. has the larger QRS complex amplitude, which always companies with more significant range differences in the waves. The QRS complex in fusion of ventricular and normal heartbeats (F. V. N.) is the fusion of normal heartbeat and ventricular flutter heartbeats (V. F.), and its deterioration will change into V. F. whose waveform is similar to sine wave, in which case cardiopulmonary resuscitation is needed for treatment.

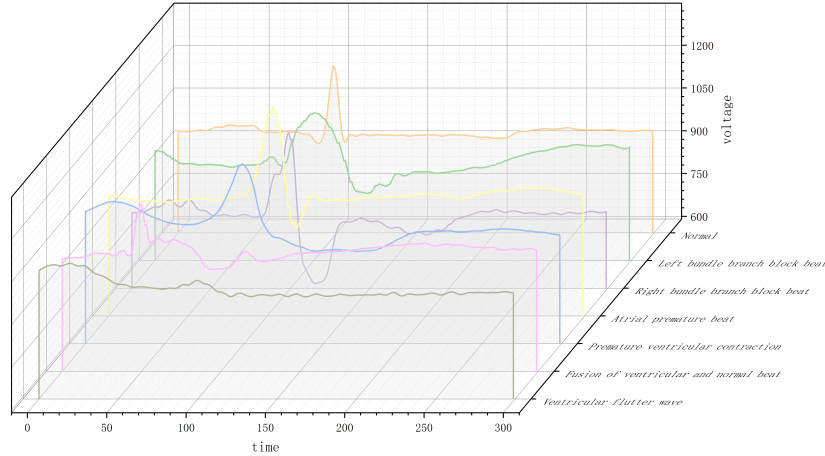


Figure 6: Schematic diagram of seven kinds of ECG signals

Figure 7 shows the point clouds in \mathbb{R}^3 for ECG signals with six pathological features. Compare Figure 2 and Figure 7, the differences of waves are reflected in the differences of local information of point clouds in \mathbb{R}^3 . Notice that the local information of the point clouds of ECG signals with diseases are significantly different from those of normal ECG signals except A. P., this may be due to the fact that A. P. is generated by atrial abnormal excitation foci in advance, and sometimes there are only P wave differences with normal ECG signals. Therefore, their local structures of Euclidean point clouds are similar.

There are also similarities among the point cloud structures of P. V. C., F. V. N., and V. F., which may be due to the fact that these three types of diseases are also generated

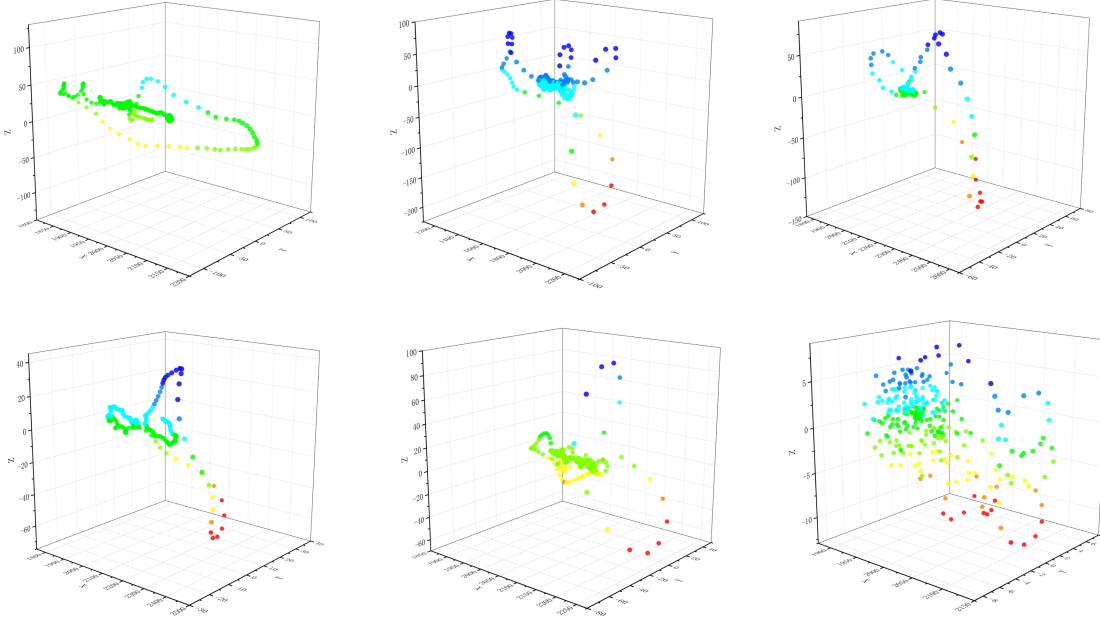


Figure 7: Point clouds of ECG signals with six pathological features in \mathbb{R}^3 after FFT embedding; the first row from left to right represents L. B. B. B., R. B. B. B., A. P.; the second row from left to right represents P. V. C., F. V. N., V. F.

from ventricular ectopic excitation foci, their pathogenesis and trend also have a certain progressive relationship. The similarities of local structures between different ECG signal point clouds also reflect the necessity of introducing WSC to describe the differences of such fine structures more accurately.

By local statistic, we change the point clouds of ECG signals with diseases into the point clouds on $SPD(3)$. The grayscale images of Wasserstein distance matrices describe the dispersion of distribution point clouds on $SPD(3)$, where black represents the zero distance and white represents the maximum distance. Local structure differences of distribution point clouds can be visually presented by Figure 3 and Figure 8.

We calculate WSC of each point to precisely characterize the differences of neighborhood information of different point clouds on $SPD(3)$. WSCs are also formed, as shown in Figure 9.

WSC sequences corresponding to seven kinds of ECG signals are almost located at $[0, 200]$, as shown in Figure 4 and Figure 9. By equation (13), it can be inferred that the neighborhood information of most points in the Euclidean point clouds do not have more than two-dimensional degradation, which shows the effectiveness of the FFT embedding method and the selected parameters.

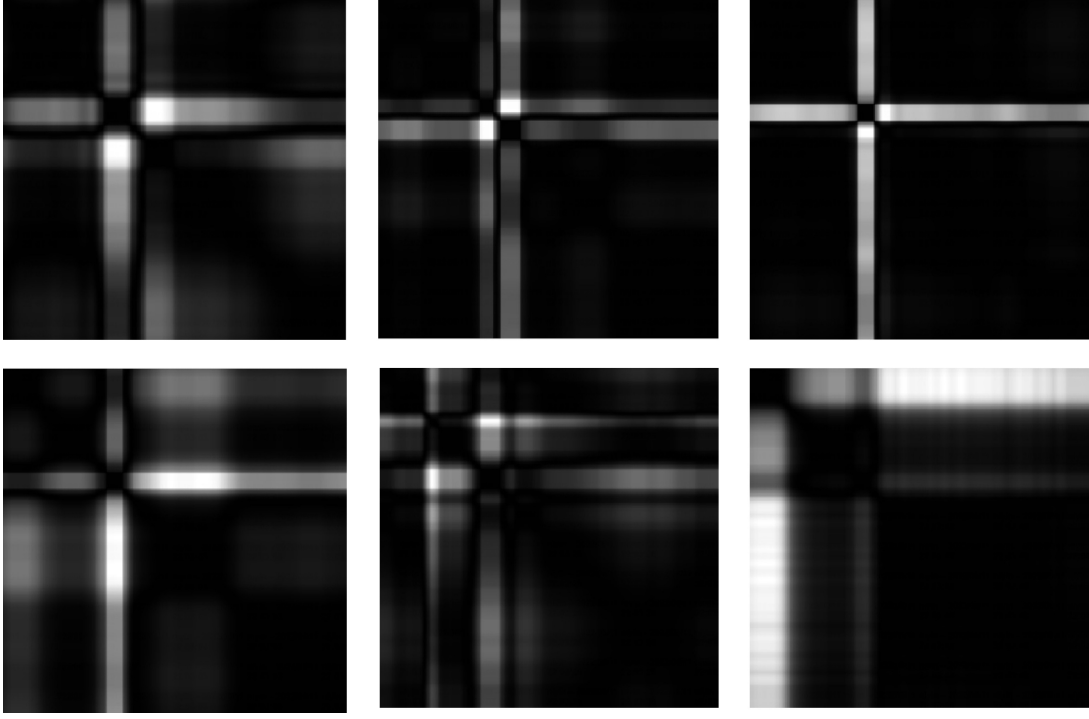


Figure 8: Grayscale image of Wasserstein distance matrices for distribution point clouds; the first row from left to right represents L. B. B. B., R. B. B. B., A. P.; the second row from left to right represents P. V. C., F. V. N., V. F.

In the histogram of normal ECG signal and A. P., their columns are evenly distributed horizontally and the columns of A. P. fluctuates more violently. The histograms of P. V. C., F. V. N. and V. F. are less evenly distributed horizontally and their fluctuation of columns are similar. The columns of L. B. B. B. and R. B. B. B. are concentrated in the smaller part of the WSC values. To identify these seven ECG signals more accurately, we calculate their WSCD.

Define Wasserstein scalar curvature dispersion plane:

$$\mathcal{D} = \{(cur_1(m, b, s), cur_2(m, b, s)) \mid -\infty < cur_1(m, b, s) < +\infty, -\infty < cur_2(m, b, s) < +\infty\}.$$

Figure 10 calculates WSCD of seven ECG signals. Transverse curvature dispersion and longitudinal curvature dispersion reveal the length and the fluctuation of QRS complex respectively. The transverse curvature dispersion gets larger with increasing width of QRS complex and the longitudinal curvature dispersion turns bigger with more violent fluctuation of QRS complex.

- QRS complex in normal ECG signal and A. P. are most regular and their transverse curvature dispersion are both largest. Notice that the lesion in the atria causes some

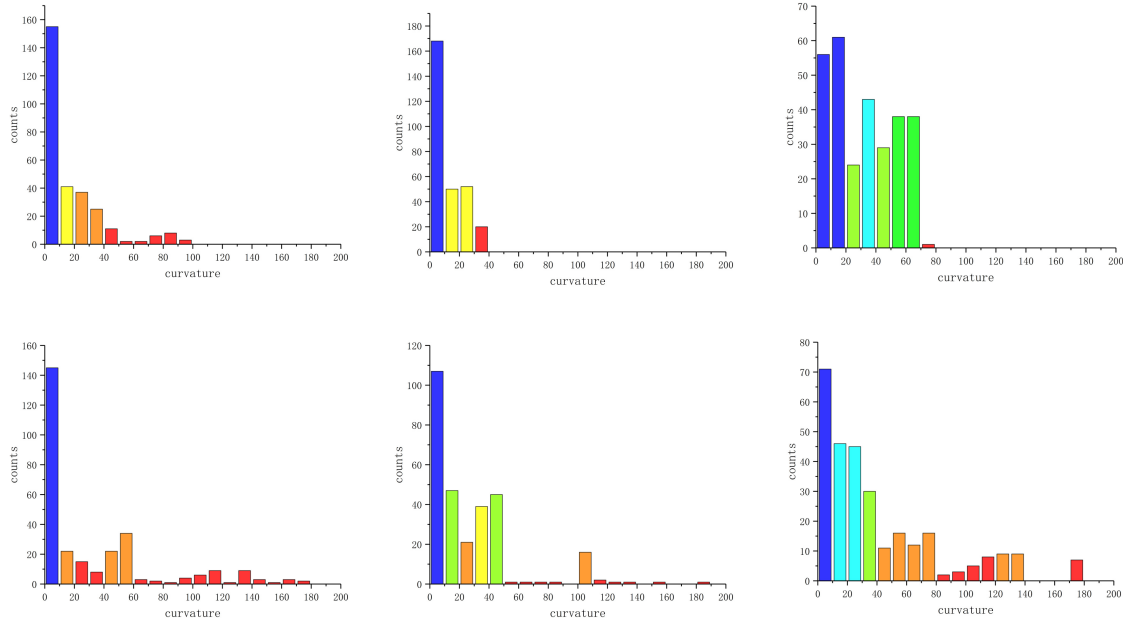


Figure 9: WSCHs of distribution point clouds of six pathological ECG signals; the first row from left to right represents L. B. B. B., R. B. B. B., A. P.; the second row from left to right represents P. V. C., F. V. N., V. F.

changes in QRS complex, hence the longitudinal curvature dispersion of A. P. is higher than normal heartbeats. Let $D_0 = (25, 200] \times [0, 25]$ denote normal status of heart and $D_1 = (25, 90] \times (25, +\infty)$ denote atrial abnormal.

- QRS complex in V. F., F. V. N. and P. V. C. are not so wide and their fluctuation gradually expand, hence the transverse curvature dispersion of these three kinds of heartbeats are moderate and their longitudinal curvature dispersion becomes bigger and bigger. Because these three kinds of heartbeats are caused by ventricular lesions, their longitudinal dispersion have some similarities. Let $D_{21} = (10, 25] \times [0, 50]$ denote V. F., $D_{22} = (10, 25] \times [40, 70]$ denote V. F. N. and $D_{23} = (10, 25] \times [60, +\infty)$ denote P. V. C.. Futhermore, let $D_2 = (10, 25] \times [0, +\infty)$ denote ventricular abnormal.
- QRS complex in L. B. B. B. and R. B. B. B. are usually widest, hence their transverse curvature dispersion are smallest. In addition, the existence of two R peaks in R. B. B. B. is more obvious than in L. B. B. B., which results in more fluctuation in QRS and the larger longitudinal curvature dispersion. Let $D_{31} = [0, 10) \times [0, 140]$ denote L. B. B. B. and $D_{32} = [0, 10) \times [100, +\infty)$ denote R. B. B. B.. In addition, let $D_3 = [0, 10) \times [0, +\infty)$ denotes bundle branch block area.

For those heartbeats which land in $D_4 = \mathcal{D} - \cup_{j=0}^3 D_j$, we think these heartbeats are from other abnormal areas. Thus, we derive a symptom description domain partition $\mathcal{D} = \cup_{j=0}^4 D_j$. Given a ECG signal T_i , the auxiliary diagnostic analysis of heart disease is as follows:

- If $cur_{T_i}(m, b, s) \in D_0$, we think T_i is normal.
- If $cur_{T_i}(m, b, s) \in D_1$, we think T_i is A. P..
- If $cur_{T_i}(m, b, s) \in D_2 \cap D_{21} - D_{22} \cup D_{23}$, we think T_i is V. F.. If $cur_{T_i}(m, b, s) \in D_2 \cap D_{22} - D_{21} \cup D_{23}$, we think T_i is V. F. N.. If $cur_{T_i}(m, b, s) \in D_2 \cap D_{23} - D_{21} \cup D_{22}$, we think T_i is P. V. C.. If $cur_{T_i}(m, b, s) \in D_{2j} \cap D_{2k}$, $1 \leq j, k \leq 3$, we think T_i has the pathological features of both D_{2j} and D_{2k} . In this case, we cannot classify T_i , but we can label it ventricular abnormal.
- If $cur_{T_i}(m, b, s) \in D_3 \cap D_{31} - D_{32}$, we think T_i is L. B. B. B.. If $cur_{T_i}(m, b, s) \in D_3 \cap D_{32} - D_{31}$, we think T_i is R. B. B. B.. If $cur_{T_i}(m, b, s) \in D_{31} \cap D_{32}$, we cannot classify T_i , but we can label it bundle branch block.
- If $cur_{T_i}(m, b, s) \in D_4$, T_i cannot be classified.

Now we give our algorithm to show how to classify the ECG signals and carry out the auxiliary diagnosis.

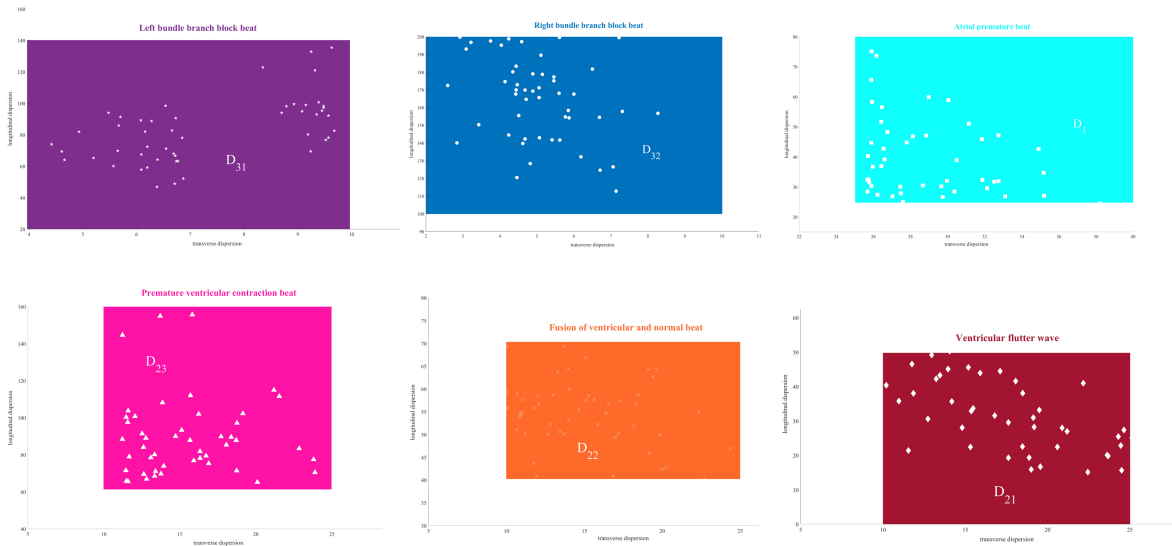


Figure 10: WSCD of seven kinds of ECG signals; the first row from left to right represents L. B. B. B., R. B. B. B., A. P.; the second row from left to right represents P. V. C., F. V. N., V. F.

3.4 WSCEC algorithm

Let $\mathcal{T} = \{T_i\}_{i=1}^N = \cup_{j=0}^r \mathcal{T}_j = \cup_{j=0}^4 \mathcal{Q}_j$ be the set of the given ECG signal where \mathcal{T}_0 is the set of normal ECG in \mathcal{T} , \mathcal{T}_j is the set of ECG with j th pathological feature in \mathcal{T} ($1 \leq j \leq r$), \mathcal{Q}_j is the original heartbeat set which is corresponding to symptom description domain D_j . Then WSCEC algorithm is shown in Algorithm 3.4.

For the output of algorithm 3.4, $\tilde{\mathcal{T}}_0$ represents the healthy heartbeat set, $\tilde{\mathcal{T}}_j$ represents the heartbeat set with j th pathological feature, $1 \leq j \leq r$, and $\tilde{\mathcal{T}}_{r+1}$ represents the unclassified heartbeat set with label of lesion area. $\tilde{\mathcal{Q}}_j$ denotes the classified heartbeat set which is corresponding to symptom description domain D_j . Thus, for a unclassified heartbeat $T_i \in \tilde{\mathcal{T}}_{r+1}$, although we cannot know the exactly type of T_i , we can also know which part of the heart is abnormal.

Algorithm 1 WSCEC algorithm

Input: ECG set \mathcal{T} ; parameter k, m, s, ϵ

Output: Classification result $\mathcal{T} = \cup_{j=0}^{r+1} \tilde{\mathcal{T}}_j \cup \tilde{\mathcal{Q}}_4 = \cup_{j=0}^4 \tilde{\mathcal{Q}}_j$

- 1: Choose standard normal ECG signal T_s
 - 2: For every ECG signal T_i in \mathcal{T} , acquire point cloud $S_F(T_i)$ after FFT embedding by equation (4)
 - 3: Acquire point cloud $S_{SPD}(T_i, k)$ of T_i and $S_{SPD}(T_s, k)$ of T_s by kNN algorithm and equation (5)
 - 4: Calculate scalar curvature at each point in $S_{SPD}(T_s, k)$ by equation (11), take b as the minimum of the max scalar curvature and $\frac{3d(d-1)}{\epsilon}$
 - 5: Calculate scalar curvature at each point in $S_{SPD}(T_i, k)$ by equation (11) and obtain curvature histogram $H(m, b)$ by equation (14)
 - 6: Calculate Wasserstein scalar curvature dispersion $cur_{T_i}(m, b, s) = (cur_1(m, b, s), cur_2(m, b, s))$ of T_i by equation (16)
 - 7: Give the classification result $\mathcal{T} = \cup_{j=0}^{r+1} \tilde{\mathcal{T}}_j \cup \tilde{\mathcal{Q}}_4 = \cup_{j=0}^4 \tilde{\mathcal{Q}}_j$ by symptom description domain partition $\mathcal{D} = \cup_{j=0}^4 D_j$
 - 8: **Output:** $\mathcal{T} = \cup_{j=0}^{r+1} \tilde{\mathcal{T}}_j \cup \tilde{\mathcal{Q}}_4 = \cup_{j=0}^4 \tilde{\mathcal{Q}}_j$
-

4 Digital Experiment

In this section, the main numerical results are introduced. The sampled data comes from MIT-BIH Arrhythmia Database [36]. We sample 5000 heartbeats with distinguishing features, including 2500 normal heartbeats (N), 1000 premature ventricular contraction heartbeats (P. V. C.), 450 left bundle branch block heartbeats (L. B. B. B.), 450 right bundle branch block heartbeats (R. B. B. B.), 200 atrial premature heartbeats (A. P.),

200 fusion of ventricular and normal heartbeats (F. V. N.) and 200 ventricular flutter heartbeats (V. F.).

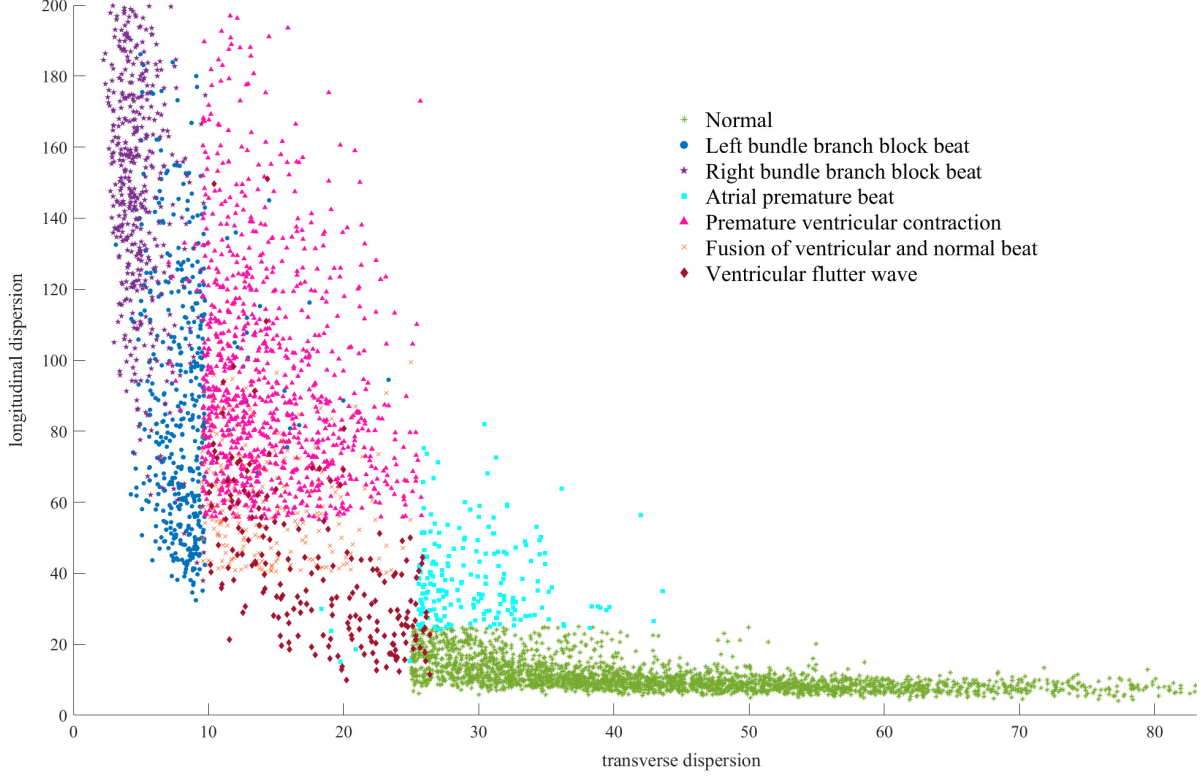


Figure 11: Wasserstein scalar curvature dispersion of seven kinds of ECG signals

Figure 11 calculates WSCD of the 5,000 segment ECG signals sampled, the parameters are $\epsilon = 0.09$, $b = \frac{3d(d-1)}{\epsilon} = 200$, $m = 1$, and $s = 0$. Note that there are overlaps between bundle branch block heartbeats and abnormal ventricular heartbeats such as F. V. N. and P. V. C., this may because all these heartbeats have widened QRS complex and some of them are indeed pretty similar. We introduce true positive rate (TPR) and noise removal rate (NRR) to show the efficiency of our symptom description domain partition.

Let $\mathcal{T} = \cup_{j=0}^4 \mathcal{Q}_j$ be the original ECG set and $\tilde{\mathcal{T}} = \cup_{j=0}^4 \tilde{\mathcal{Q}}_j$ be the set after classification. Then for all $0 \leq j \leq 4$,

$$\begin{aligned} \text{TPR}_j &= \frac{|\tilde{\mathcal{Q}}_j \cap \mathcal{Q}_j|}{|\mathcal{Q}_j|}, \\ \text{NRR}_j &= 1 - \frac{|\tilde{\mathcal{Q}}_j \cap \cup_{k \neq j} \mathcal{Q}_k|}{|\cup_{k \neq j} \mathcal{Q}_k|}, \end{aligned} \tag{18}$$

where $|\cdot|$ denotes the cardinality or size of a finite set.

TPR_j describes the accuracy of original ECG signals with lesion area j preserved

by the new classification. NRR_j represents the success rate of removing ECG signals except j . It can be intuitively understood that higher TPR and NRR represent better classification ability. Table 1 shows the classification accuracy of symptom description domain partition. Intuitively, the normal ECG can be very accurately separated from other heartbeats with pathological features.

Table 1: Classification result of symptom description domain partition

ECG type	Normal	Atrial abnormal	Ventricular abnormal			Bundle branch block		Unclassified
	N	A. P.	P. V. C.	F. V. N.	V. F.	L. B. B. B.	R. B. B. B.	Null
Original size	2500	200	1400			900		0
Classified size	2513	212	1305			970		0
TPR	99.96%	95.50%	91.36%			97.78%		0
NRR	99.44%	99.56%	99.35%			97.80%		0

To show the classification results of each specific disease and the validity of symptom description domain partition, we use principal component analysis (PCA) to obtain the confidence elliptic region [37], as shown in Figure 12. Notice that almost every confidence elliptic region is contained in the corresponding symptom description domain, hence the selection of our symptom description domain partition has strong robustness.

Although the results from normal ECG signals are basically identical, ECG signals with different pathological features tend to have different degrees of change and ECG signals may vary even if they share same pathological feature. Thus, firstly, we infer the location of cardiac abnormalities such as atrium, ventricle and atrioventricular bundle. Secondly, we give the reference diagnostic results. For those ECG signals which we can infer the location of cardiac abnormality but cannot make sure the exactly disease, doctors needs to make further diagnosis. Furthermore, we can estimate the severity of pathology according to the longitudinal dispersion.

5 Conclusions and Future Works

In this paper, a novel ECG assisted classification algorithm based on Wasserstein scalar curvature is proposed. By introducing Wasserstein scalar curvature, WSCEC algorithm more accurately describes the neighborhood information differences of point clouds obtained after FFT embedding, and realizes the classification of seven kinds of single-lead

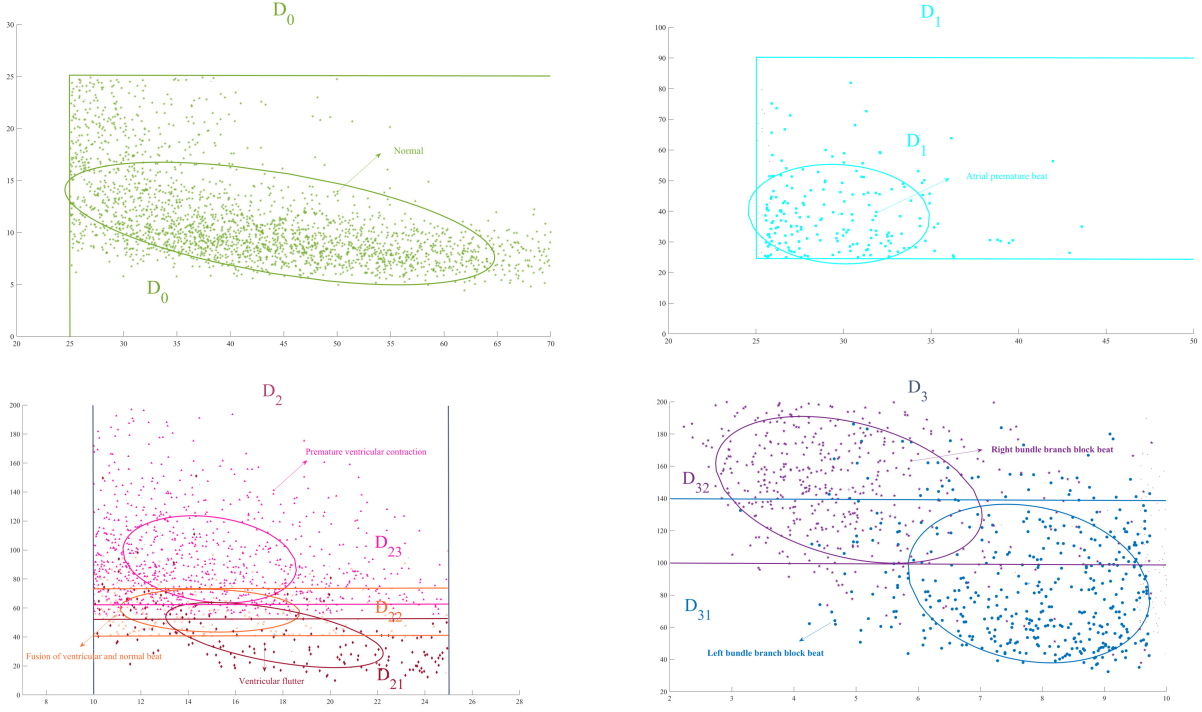


Figure 12: Principal component analysis result

ECG with different pathological features. The accuracy and interpretability of WSCEC algorithm are strong.

WSCEC algorithm is an original attempt to incorporate geometric invariants into medical research, and it is expected to be further applied to other big databases and the standard 12-lead ECG auxiliary diagnosis. Meanwhile, WSCEC algorithm can also be applied to a variety of signal research such as signal identification and Electroencephalogram (EEG) analysis. How to choose a more reasonable signal embedding way and how to further combine with topological data analysis to comprehensively investigate the signal from the whole and local to get more efficient algorithms need further research.

References

- [1] World Health Organization. The top 10 causes of death. <https://www.who.int/news-room/fact-sheets/detail/the-top-10-causes-of-death>.
- [2] M.D. Aswini Kumar. ECG simplified. LifeHugger. [010-02-11].
- [3] J.K. Cooper. Electrocardiography 100 years ago. Origins, pioneers, and contributors. The New England Journal of Medicine, 315(1986), 461–464.

- [4] I. Christov, G. Gómez-Herrero, V. Krasteva, I. Jekova, A. Gotchev, K. Egiazar-ian. Comparative study of morphological and time-frequency ECG descriptors for heartbeat classification, 28(2006), 876-887.
- [5] C. Ye, B.V. Kumar, M.T. Coimbra. Heartbeat classification using morphological and dynamic features of ECG signals. IEEE Transactions on Biomedical Engineering, 59(2012), 2930-2941.
- [6] S. Banerjee, M. Mitra. Application of cross wavelet transform for ECG pattern analysis and classification. IEEE transactions on instrumentation and measurement, 63(2013), 326-333.
- [7] R. He, K. Wang, N. Zhao, Y. Liu, Y. Yuan, Q. Li, H.Zhang. Automatic detection of atrial fibrillation based on continuous wavelet transform and 2d convolutional neural networks. Frontiers in physiology, 9(2018), 1206.
- [8] X. Hua, Y. Ono, L. Peng, Y. Cheng and H. Wang. Target Detection Within Nonhomogeneous Clutter Via Total Bregman Divergence-Based Matrix Information Geometry Detectors. IEEE Transactions on Signal Processing, 69(2021), 4326-4340.
- [9] M. Richter, T. Schreiber. Phase space embedding of electrocardiograms. Physical Review E, 58(1998), 6392.
- [10] C.K. Chen, C.L. Lin, S.L. Lin, Y.M. Chiu, C.T. Chiang. A chaotic theoretical approach to ECG-based identity recognition. IEEE Computational Intelligence Magazine, 9(2014), 53-63.
- [11] U. Desai, R.J. Martis, U.R. Acharya, C.G. Nayak, G. Seshikala, R. SHETTY K. Diagnosis of multiclass tachycardia beats using recurrence quantification analysis and ensemble classifiers. Journal of Mechanics in Medicine and Biology, 16(2016), 1640005.
- [12] L.Y. Di Marco, D. Raine, J.P. Bourke, P. Langley. Recurring patterns of atrial fibrillation in surface ECG predict restoration of sinus rhythm by catheter ablation. Computers in biology and medicine, 54(2014), 172-179.
- [13] Y. Gong, Y. Lu, L. Zhang, H. Zhang, Y. Li. Predict defibrillation outcome using stepping increment of poicare plot for out-of-hospital ventricular fibrillation cardiac arrest. BioMed research international, 2015.

- [14] T. Stamkopoulos, K. Diamantaras, N. Maglaveras, M. Strintzis. ECG analysis using nonlinear PCA neural networks for ischemia detection. *IEEE Transactions on Signal Processing*, 46(1998), 3058-3067.
- [15] J. Li. Detection of premature ventricular contractions using densely connected deep convolutional neural network with spatial pyramid pooling layer. *arXiv preprint, arXiv:1806.04564*, 2018.
- [16] W. Lu, J. Shuai, S. Gu, and J. Xue. Method to Annotate Arrhythmias by Deep Network. 2018 IEEE International Conference on Internet of Things (iThings) and IEEE Green Computing and Communications (GreenCom) and IEEE Cyber, Physical and Social Computing (CPSCoM) and IEEE Smart Data (SmartData). IEEE, 2018, 1848-1851.
- [17] Y. Yan, X. Qin, Y. Wu, N. Zhang, J. Fan, L. Wang. A restricted Boltzmann machine based two-lead electrocardiography classification. 2015 IEEE 12th international conference on wearable and implantable body sensor networks (BSN). IEEE, 2015, 1-9.
- [18] B.A. Fraser, M.P. Wachowiak, R. Wachowiak-Smolíková(2017, April). Time-delay lifts for physiological signal exploration: an application to ECG analysis. In 2017 IEEE 30th Canadian Conference on Electrical and Computer Engineering (CCECE). IEEE, 2017, 1-4.
- [19] B. Safarbali, S.M.R.H. Golpayegani. Nonlinear dynamic approaches to identify atrial fibrillation progression based on topological methods. *Biomedical Signal Processing and Control*, 53(2019), 101563.
- [20] P.S. Ignacio, C. Dunstan, E. Escobar, et al. Classification of single-lead electrocardiograms: TDA informed machine learning. 2019 18th IEEE International Conference On Machine Learning And Applications (ICMLA). IEEE, 2019, 1241-1246.
- [21] G. Graff, B. Graff, P. Pilarczyk, et al. Persistent homology as a new method of the assessment of heart rate variability. *Plos one*, 16(2021), e0253851.
- [22] M. Dindin, Y. Umeda, F. Chazal. Topological Data Analysis for Arrhythmia Detection Through Modular Neural Networks. *Canadian Conference on AI*, 2020, 177-188.
- [23] Y. Ni, F. Sun, Y. Luo, Z. Xiang, H. Sun. A Novel Heart Disease Classification Algorithm based on Fourier Transform and Persistent Homology. 2022 IEEE Inter-

- national Conference on Electrical Engineering, Big Data and Algorithms (EEBDA 2022), 2022.
- [24] U. Bauer. Ripser: efficient computation of Vietoris–Rips persistence barcodes. *J Appl. and Comput. Topology* 5, 2021, 391–423.
 - [25] Y. Rubner, C. Tomasi, L. Guibas. A metric for distributions with applications to image databases. *Sixth International Conference on Computer Vision (IEEE Cat. No. 98CH36271)*. IEEE, 1998, 59-66.
 - [26] E. Massart, P.A. Absil. Quotient Geometry with Simple Geodesics for the Manifold of Fixed-rank Positive-semidefinite Matrices. *SLAM Journal on Matrix Analysis and Applications*, 41(2020), 171-198.
 - [27] Y. Luo, S. Zhang, Y. Cao, H. Sun. Geometric Characteristics of the Wasserstein Metric on $\text{SPD}(n)$ and Its Applications on Data Processing. *Entropy*, 23(2021), 1214.
 - [28] C. Givens, R.M. Shortt. A Class of Wasserstein Metrics for Probability Distributions. *Michigan Mathematical Journal*, 31(1984), 231-240.
 - [29] S. Butterworth. On the theory of filter amplifiers. *Wireless Engineer*, 7(1930), 536-541.
 - [30] A. Ward. A General Analysis of Sylvester’s Matrix Equation. *International Journal of Mathematical Education in Science and Technology*, 1991.
 - [31] F. Takens. Detecting Strange Attractors in Turbulence. *Dynamical Systems and Turbulence*, 1981, 366-381.
 - [32] M.B. Kennel, R. Brown, H.D.I. Abarbanel. Determining embedding dimension for phase-space reconstruction using a geometrical construction. *Physical review A*, 45(1992), 3403.
 - [33] A.M. Fraser, H.L. Swinney. Independent coordinates for strange attractors from mutual information. *Physical review A*, 33(1986), 1134.
 - [34] G. Darbellay, I. Vajda. Estimation of the information by an adaptive partitioning of the observation space. *IEEE Transactions on Information Theory*, 45(1999), 1315-1321.

- [35] A. Kraskov, H. Stögbauer, P. Grassberger. Estimating mutual information. *Physical review E*, 69(2004), 066138.
- [36] L. Maršánová, A. Němcová, R. Smíšek, T. Goldmann, M. Vitek, L. Smital. Automatic Detection of P Wave in ECG During Ventricular Extrasystoles. *World Congress on Medical Physics and Biomedical Engineering 2018: Springer, Singapore*, 2018, 381-385.
- [37] J.P. Stevens. *Applied multivariate statistics for the social sciences*. Routledge, 2012.